Talanta 85 (2011) 1253–1259

Contents lists available at ScienceDirect

Talanta

journal homepage: www.elsevier.com/locate/talanta

Fast heating induced impulse halogenation of refractory sample components in electrothermal atomic absorption spectrometry by direct injection of a liquid halogenating agent

Krisztina György[a], Zsolt Ajtony[b], Katleen Van Meel[c], René Van Grieken[c], Aladár Czitrovszky[a], László Bencs[a,c,*]

[a] Research Institute for Solid State Physics and Optics (RISSPO), Hungarian Academy of Sciences, P.O. Box 49, H-1525 Budapest, Hungary
[b] Institute of Food Science, University of West Hungary, Lucsony u. 15-17, H-9200 Mosonmagyaróvár, Hungary
[c] Micro and Trace Analysis Centre, Department of Chemistry, University of Antwerp, Universiteitsplein 1, B-2610 Antwerp, Belgium

ARTICLE INFO

Article history:
Received 16 December 2010
Received in revised form 5 May 2011
Accepted 17 May 2011
Available online 26 May 2011

Keywords:
Halogenating precursor
Graphite furnace atomic absorption spectrometry
Electrothermal vaporization and atomization
Memory effect
Halocarbon-assisted clean-out
GFAAS

ABSTRACT

A novel electrothermal atomic absorption spectrometry (ETAAS) method was developed for the halogenation of refractory sample components (Er, Nd and Nb) of lithium niobate ($LiNbO_3$) and bismuth tellurite (Bi_2TeO_5) optical single crystals to overcome memory effects and carry-over. For this purpose, the cleaning step of a regular graphite furnace heating program was replaced with a halogenation cycle. In this cycle, after the graphite tube cooled to room temperature, a 20 μL aliquot of liquid carbon tetrachloride (CCl_4) was dispensed with a conventional autosampler into the graphite tube. The CCl_4 was partially dried at 80 °C under the mini-flow (40 $cm^3\,min^{-1}$) condition of the Ar internal furnace gas (IFG), then the residue was decomposed (pyrolyzed) by fast furnace heating at 1900–2100 °C under interrupted flow of the IFG. This step was followed by a clean-out stage at 2100 °C under the maximum flow of the IFG. The advantage of the present method is that it does not require any alteration to the graphite furnace gas supply system in contrast to most of the formerly introduced halogenation techniques.

The effectiveness of the halogenation method was verified with the determination of Er and Nd dopants in the optical crystals. In these analyses, a sensitivity decrease was observed, which was likely due to the enhanced deterioration of the graphite tube surface. Therefore, the application of mathematical correction (resloping) of the calibration was also required. The calibration curves were linear up to 1.5 and 10 μmol L^{-1} for Er and Nd, respectively. Characteristic masses of 18 and 241 pg and the limit of detection (LOD) values of 0.017 and 0.27 μmol L^{-1} were found for Er and Nd, respectively. These LOD data correspond to 0.68 μmol mol^{-1} Er and 11 μmol mol^{-1} Nd in solid bismuth tellurite samples. The analytical results were compared with those obtained by a conventional ETAAS method and validated with X-ray fluorescence spectrometry analysis.

1. Introduction

For the past decades, application of halogenation to overcome carry-over or memory effects has gained increasing attention in electrothermal atomic absorption spectrometry (ETAAS) [1–7] and in electrothermal vaporization (ETV) coupled techniques [8–14]. Halogenating agents (e.g., halocarbons) promote the vaporization of refractory species (e.g., transition metals, oxides, carbides and silicides) by forming their more volatile compounds in the graphite furnace [1]. Halocarbons can also increase the transport efficiency of several sample components in ETV-coupled techniques, for instance, through aerosol formation [10].

As early as 1974, Kántor et al. [1] applied diluted carbon tetrachloride (CCl_4) vapor at ~2000 °C for 2–3 min in a graphite furnace atomizer, operated at continuous sample introduction, to get rid of carbide forming metal impurities (e.g., Al and Ti) deposited after each analytical cycle. For halocarbon introduction, the internal furnace gas (IFG) at a flow-rate of 0.5 L min^{-1} was purged through a gas-washer flask containing a few mL of CCl_4.

Later, Welz and Schlemmer [2] mixed 1% (v/v) Freon-23 (CHF_3) into the IFG (Ar) to reduce memory effects in the determination of Mo. This method allowed the temperature of the clean-out step to be reduced, therefore, extended the lifetime of the graphite tubes by a factor of two. Dočekal and Krivan [3] applied CCl_4 and carbon

* Corresponding author at: Research Institute for Solid State Physics and Optics (RISSPO), Hungarian Academy of Sciences, P.O. Box 49, H-1525 Budapest, Hungary. Tel.: +36 1 392 2222x1684; fax: +36 1 392 2223.
E-mail address: bencs@szfki.hu (L. Bencs).

0039-9140/$ – see front matter © 2011 Elsevier B.V. All rights reserved.
doi:10.1016/j.talanta.2011.05.028

tetrafluoride (CF_4) mixed into the IFG (Ar) during the cleaning after-treatment stage in ETAAS for the removal of the interfering Mo matrix. Sample masses up to 0.1 mg of Mo, introduced as metal, oxide, or silicide, could be quickly volatilized. Interference effects caused by residual halogenated pyrolysis products retained in the atomizer after the CF_4 treatment could be effectively eliminated using a mixture of H_2 and Ar as the IFG in the atomization stage.

Knutsen et al. [4] mixed 2% (v/v) CHF_3 to the Ar purge gas at the cleaning step, or at the end of the atomization stage for the determination of Dy in serum and blood samples. They observed that any increase in the concentration of Freon-23 during the cleaning step caused a sensitivity decrease in the subsequent analytical cycle. Scaccia and Zappa [5] used 1% (v/v) CHF_3 mixed to the Ar IFG for the complete evaporation of an Al matrix without any loss of the analyte (Fe).

Heinrich and Matschat [6] premixed 1% Freon in various forms (either CCl_2F_2, $CHClF_2$, or CHF_3) into the IFG to minimize carbide formation of Cr, Mo, Ti and V in the analysis of digested ceramics. The introduction of Freon was optimal during the atomization and/or clean-out steps, implying that in the other furnace program steps an Ar-H_2 mixture had to be used for purging the graphite furnace. This purging most likely served to get rid of the residual Freon compounds, retained in the atomizer after halogenation.

Matoušek and Powell [7] used a gas syringe to introduce manually a 1:5 (v/v) mixture of Cl_2 and N_2 into the graphite furnace atomizer through a drilled gas introduction port, in order to aid the vaporization of refractory compounds of Cr and V. Later on, a similar approach was adapted to the ETV inductively coupled plasma optical emission spectrometry (ICP-OES) technique, i.e., a 1 mL of Cl_2–Ar mixture was injected from a glass flask into the ETV device to facilitate the low-temperature vaporization of Cr, Ti, V, W and Zr [8].

Following on the ETV-related literature, Kirkbright and Snook [9] applied CCl_4–Ar mixtures to promote the volatilization of refractory compounds of B, Cr, Mo, W and Zr from a graphite rod ETV unit into an ICP-OES system. As the ETV heated up to the vaporization temperature, the particular halocarbons decomposed to C and active halogen radicals, which halogenated the species of interest. Kántor [10] applied CCl_4 vapors by carrier volatilization of the liquid in a wash-bottle by the IFG (Ar) in ETV-ICP-OES and compared the co-volatilization and selective volatilization approaches of As, Cd, Pb, Se and Hg in alkaline and alkaline earth metal matrices. A nearly simultaneous vaporization of 16 elements using chlorination with CCl_4 vapor at 2100 °C could be performed for a multielement ETV-ICP-OES analysis. A similar technique was also applied to assist the vaporization of Er and Nd dopants in the presence of bismuth tellurite crystal matrix in ETV-ICP-OES [11]. The halogenation and the aerosol transport from the ETV device to the detection source were accomplished within 30 s at a relatively low vaporization temperature (1760 °C).

Peng et al. [12] utilized polytetrafluoroethylene (PTFE) emulsion to assist the vaporization of silicon carbide slurry in ETV-ICP-OES, to determine Al, Cr, Cu, Fe and V trace impurities. The vaporization of 100 μg of the matrix was accomplished within 60 s at a pyrolysis temperature of 800 °C without any considerable analyte loss. Similar fluorination approaches to slurries of silicon nitride and aluminum oxide ceramics have been developed for the ETV-ICP-OES determination of Cr, Cu, Fe and V traces [13,14].

These gaseous phase chemical additives/modifiers in ETAAS were thoroughly reviewed by Tsalev et al. [15,16], while the ETV-related aspects of halogenation were reviewed in details by Kántor [17] and formerly by Nickel and Broekaert for ceramic powders [18].

Lithium niobate ($LiNbO_3$) and bismuth tellurite (Bi_2TeO_5) are important laser crystals in which rare earth element (REE) dopants, such as Er and/or Nd are utilized to influence certain optical properties (e.g., Refs. [19,20]). These crystals that are produced in the Crystal Physics Laboratory of RISSPO are analyzed by ETAAS. The ETAAS literature [21–23] reports that in graphite furnaces Er and Nd analytes tend to form heavy volatile, refractory compounds, whose insufficient degree of vaporization can result in memory effects and carry-over. These unwanted effects can be expected to be more serious in the presence of a refractory matrix, such as the $LiNbO_3$.

The drawbacks of most of the above mentioned halogen introduction methods are the necessity of alterations on the furnace gas supply system and/or the graphite furnace itself. An alternative and simple approach for halogen introduction may be the application of a common ETAAS autosampler to dispense halocarbons (e.g., CCl_4) in liquid form directly into the graphite furnace. However, a typical, well reproducible sample volume of 20 μL CCl_4 (i.e., 0.2 mmol CCl_4 at room temperature (RT)) is at a high excess compared to the sample residues remaining after a common drying cycle (e.g., 0.2 μmol $LiNbO_3$ from a typical 0.01 mol L^{-1} sample solution of 20 μL volume). This halocarbon excess may cause sensitivity decrease in subsequent analytical cycles and also a vigorous corrosion of the surface of the graphite tube. Consequently, the amount of the dispensed halogenation agent should be reduced in the furnace before the halogenation process. Its required amount can be obtained, for instance, by an incomplete drying of the halocarbon droplet dispensed into the graphite furnace. Then the next step would be the halogenation, which requires the fast heating of the graphite furnace to attain expansion of the halocarbon vapor.

Holcombe [24] studied the expulsion of matrix vapors in an end-heated graphite tube atomizer under fast heating and observed analyte/matrix losses at the tube ends, due to vapor expansion. On the base of his study, it is expected that the residue of the chlorinating agent expands and fills in the whole volume of the graphite tube, when using fast heating and interrupted flow of the IFG, which exhibits the possibility of an efficient removal of the refractory sample components.

In the framework of this study, a novel method of liquid CCl_4-assisted halogenation is developed for the removal of the refractory sample components from the graphite tube by an extended clean-out program. The proposed method is applied for the ETAAS analysis of optical laser crystals. The results were compared to those obtained by a conventional ETAAS method and validated with energy dispersive X-ray fluorescence (EDXRF) analysis.

2. Experimental

2.1. ETAAS instrumentation

All the ETAAS experiments were performed on a Carl-Zeiss model AAS-3 (Jena, Germany) atomic absorption spectrometer, equipped with an end-heated EA-3 (Carl-Zeiss) graphite tube electrothermal atomizer. Peak height (A_p) and integrated absorbance (A_{int}) signals were measured at the analytical lines of Er 400.8 nm and Nd 492.4 nm, each with a spectral bandpass of 0.2 nm. Hollow cathode lamps of Er and Nd were operated at 7 and 12 mA current, respectively. A tungsten halogenide lamp was used for continuum source background (BG) correction. High purity Ar (4N5) was supplied as the furnace purge gas with an external flow rate of 1000 cm^3 min^{-1}. Sample/standard aliquots of 20 μL were dispensed with an MPE (MLW, Germany) autosampler onto the wall of pyrolytically coated graphite tubes (Electrokohle, Lichtenberg, Germany). The samples were weighed on a Kern model 770-14 (Balingen, Germany) electronic analytical balance. The data of the transient absorbance signals were collected by the built-in computer of the spectrometer and subsequently written out by an Endim 621.04 (Schlotheim, Germany) chart recorder. The signal integration time was 5 s, if not stated otherwise. Three replicates

Table 1
Conventional graphite furnace heating program for the determination of Er and Nd.

Step	Temperature (°C)	Ramp (°C s^{-1})	Hold (s)	Internal gas flow rate (cm^3 min^{-1})
Drying	100	5	25	160
Pyrolysis[a]	1000/1200[b]	100	20	160
Atomization	2600	2650[c]	5[d]	40
Clean-out	2650	2650[c]	2	280

[a] Baseline measured at the end of this step for 3 s.
[b] Pyrolysis temperature: 1000 °C and 1200 °C for matrix-free standards/Bi_2TeO_5 and $LiNbO_3$, respectively.
[c] Maximum power heating.
[d] Signal integration for 5 s.

of each sample/standard solution were measured. The graphite furnace heating program of the conventional ETAAS method is presented in Table 1.

2.2. Materials and methods

All the chemicals were of analytical grade or better quality (supplier: Reanal, Budapest, Hungary, if not stated otherwise). For the dilution of the sample/standard solutions, ion-exchanged and doubly distilled water was applied. Stock and standard solutions were prepared as described in details in Ref. [11]. The optical crystals were grown as reported elsewhere [25,26]. The samples were cut from various parts of the crystal bulk. These samples were ground in agate mortars, specifically used only for one crystal type to avoid cross contamination of matrices. Each powdered $LiNbO_3$ sample (weight: ~0.147 g) was digested in a Pt crucible with a mixture of 2 mL of 96% (m/m) H_2SO_4 plus 2 g KCl on heating with a Bunsen burner. After solidification and cooling of the melt, 10 mL of 1.0 mol L^{-1} triammonium citrate (TAC) was applied to dissolve the digested sample. Then the sample solution was made up to 100 mL in a volumetric flask. The TAC stock solution was prepared from Suprapur grade ammonia and citric acid (Merck, Darmstadt, Germany). For Bi_2TeO_5 crystals, the dissolution method is described in details elsewhere [27–31]. Three replicates were weighed and digested from each crystal sample.

For halogenation purposes, a 20 μL aliquot of CCl_4 liquid was injected by the autosampler into the graphite tube, when the tube cooled to RT after a modified analytical cycle, in which the clean-out step was omitted. In these interim cleaning cycles, an incomplete drying of the CCl_4 liquid and its evaporation under interrupted flow of the IFG were applied, which was followed by a clean-out step with the maximum flow rate of the IFG to expel the halogen containing compounds. The graphite furnace heating program extended with the CCl_4-assisted halogenation is presented in Table 2.

During the analysis, first the standard solutions were measured, then the CCl_4-assisted clean-out was applied, followed by a blank run. These calibration steps were repeated two times. After calibration, each sample was measured three times, then resloping was performed, along with the CCl_4-assisted step and one blank run. The resloping of the calibration was made by measuring one of the standards of medium concentration. The sample solutions were measured either without dilution (Nd), or after 5-fold (Er, Nd), or 50-fold (Er) dilution. Two-tailed *F*- and *t*-tests at the 95% confidence level were applied to compare the analytical results acquired with the different analytical methods.

2.3. EDXRF analysis

For the EDXRF analysis, an Epsilon 5 (PANalytical, Almelo, The Netherlands) high-energy spectrometer with Cartesian, polarizing geometry was applied. This instrument is equipped with a 600 W Gd-anode and a high purity Ge-detector. The analysis was performed under vacuum and by rotating the samples with a spinner. The samples were irradiated with a W target (under 100 kV and 6 mA acceleration conditions) during an acquisition time of 1000s.

Samples were prepared by injecting 300 μL of the sample/standard solutions, prepared as above, to the middle of an around 70 mm × 73 mm piece of 3511-Kapton® thin film (8 μm) for XRF (SPEX CertiPrep, Metuchen, NJ, USA). The films with the droplets of the solutions were left on standing under a laminar flow exhaust unit until they became completely dry. After then, each film was placed into a sample holder cup with another Kapton film on top of it, carefully positioned to get the dry residue at the middle of the cup, and then fixed with the insert of the sample holder. Calibration was performed against matrix-matched standards.

3. Results and discussion

3.1. Vaporization studies with a conventional graphite furnace heating program

3.1.1. Memory effects of Er and Nd without matrix

The memory effect of Er and Nd was studied using the conventional graphite furnace program (Table 1). As can be seen in Fig. 1, a considerable memory effect (e.g., more than the 10% of the original Er signal) was found after 10 subsequent runs, when dispensing an acidic Er standard. This memory signal decreased to

Table 2
Graphite furnace heating program for the determination of Er and Nd with CCl_4-assisted clean-out.

Step	Temperature (°C)	Ramp (°C s^{-1})	Hold (s)	Internal gas flow rate (cm^3 min^{-1})
Drying (sample)	100	5	25	160
Pyrolysis[a]	1000/1200[b]	100	20	160
Atomization (cooling to RT, then dispension of CCl_4)	2600	2650[c]	5[d]	40
Drying (CCl_4)	80	20	10	40
Vaporization (halogenation)	1900/2100[e]	1000	8	0
Clean-out	1900/2100[e]	0[c]	15	280

RT – room temperature.
[a] Baseline measured at the end of this step for 3 s.
[b] Pyrolysis temperature: 1000 °C and 1200 °C for matrix-free standards/Bi_2TeO_5 and $LiNbO_3$, respectively.
[c] Maximum power heating.
[d] Signal integration for 5 s.
[e] Vaporization/clean-out temperature: 1900 °C and 2100 °C for Nd and Er, respectively.

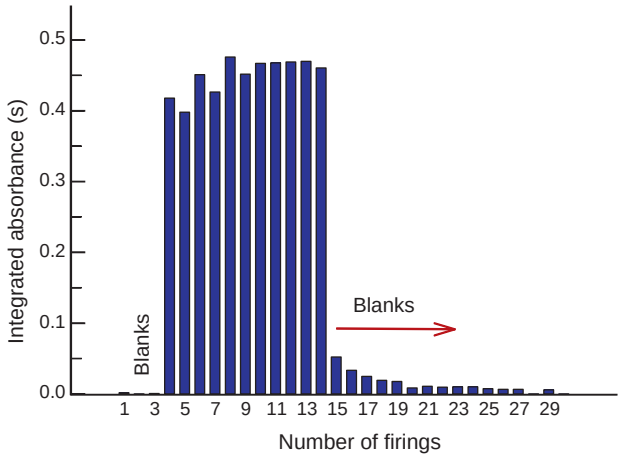

Fig. 1. Integrated absorbance signals of 1 μmol L^{-1} Er in 0.8 mol L^{-1} HCl (steps 4–14) and subsequent blank runs with unloaded furnace (steps 15–29) using a conventional graphite furnace heating program.

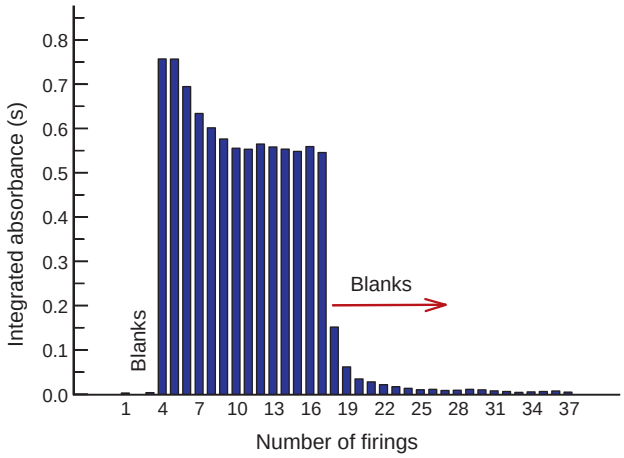

Fig. 3. Integrated absorbance signals of 1 μmol L^{-1} Er in the presence of 0.01 mol L^{-1} lithium niobate (steps 4–17) and subsequent blank runs with unloaded furnace (steps 18–37) using a conventional graphite furnace heating program.

the level of the regular blank only after 15 subsequent firings of the unloaded graphite tube. Due to the application of the highest allowable atomization and clean-out temperature (2650 °C), the lifetime of the graphite tubes decreased dramatically. A similar memory effect was experienced for Nd (Fig. 2). The memory signal reached as high as 10% of the A_{int} signal, measured in the previous analytical cycle, and it decreased rather slowly, following an exponential function.

3.1.2. *Vaporization of Er and Nd in the presence of various matrices*

3.1.2.1. Lithium niobate. In this series of the measurements, as a first step, a 0.01 mol L^{-1} $LiNbO_3$ matrix was applied in the Er solution. Using the same experimental conditions as mentioned above for aqueous standards, the Er signal was constant in the first two measurements, then decreased significantly in the subsequent 3–7 runs and it remained nearly constant again (Fig. 3). Memory signals measured in subsequent runs (i.e., without dispensing any solution) were approximately three times higher (e.g., A_{int}(blank) = 0.15 s) compared to the case when no matrix was present (Fig. 1). This amplified memory effect is probably due to the presence of refractory carbide/oxide forming matrix ($LiNbO_3$), and due to this, the analyte could be evaporated at a lower rate. This memory signal was also showing an exponential decay by the increasing number of blank runs.

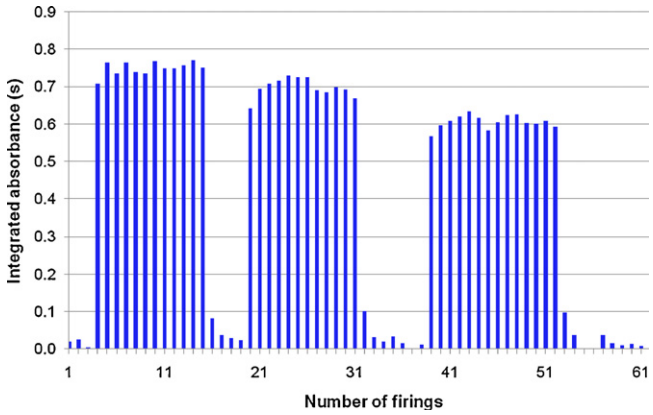

Fig. 2. Integrated absorbance signals of 10 μmol L^{-1} Nd in 0.8 mol L^{-1} HCl (steps 4–15, 20–31, 39–52) and (subsequent) blank runs with unloaded furnace (steps 1–3, 16–19, 32–38, 53–61) using a conventional graphite furnace heating program.

The change in the extent of BG absorbance (peak height) of $LiNbO_3$ during its co-vaporization with 2 μmol L^{-1} Er was also observed (Fig. 4). As can be seen, the increase in the number of firings rapidly increased the BG absorbance by more than two times. This means that more matrix salts were retained in the furnace in line with the deterioration of the graphite surface. On the other hand, the subsequent blank runs showed near baseline levels of the BG absorbance (Fig. 4). It is to be noted that the problems caused by the presence of high, structured background originating from the vaporization of molecular forms of sample components can be overcome by the application of either Zeeman [32] or Smith–Hieftje [33] BG correction.

Similarly high memory signals were acquired in the case of Nd applied with $LiNbO_3$ matrix as observed for Er above, although the matrix concentration was much lower (0.0005 mol L^{-1}) than in the case of Er. The memory signal of Nd was decreasing, but after some firings it remained rather fluctuating, which likely means that in the presence of the $LiNbO_3$ matrix, Nd is more bound to the graphite than Er. When the concentration of $LiNbO_3$ was increased to 0.001 mol L^{-1} (Fig. 5), the memory signal of Nd increased to practically 1.5-fold of the value observed with the lower matrix content (0.0005 mol L^{-1}). Moreover, the deterioration of the A_{int} signal in

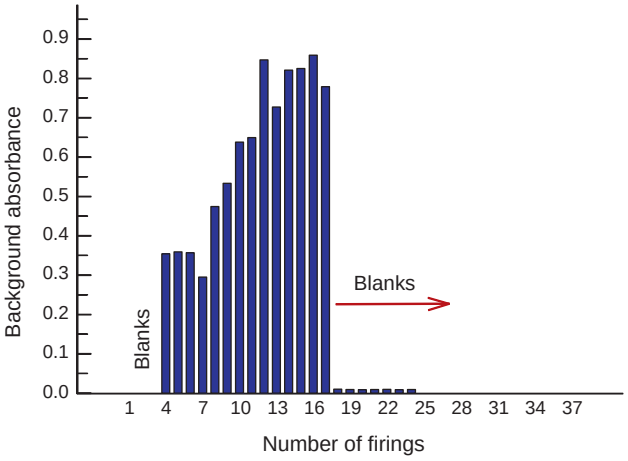

Fig. 4. Background absorbance (peak height) of 0.01 mol L^{-1} lithium niobate (with 1 μmol L^{-1} Er) measured at the Er 400.8 nm line (steps 4–17) and subsequent blank runs with unloaded furnace (steps 18–37) using a conventional graphite furnace heating program.

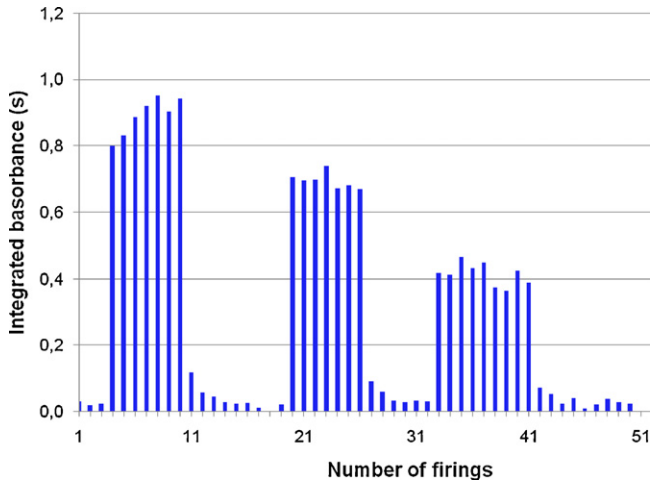

Fig. 5. Integrated absorbance signals of 10 μmol L^{-1} Nd in the presence of 0.001 mol L^{-1} lithium niobate and 0.05 mol L^{-1} TAC obtained with the conventional furnace heating program (steps 4–10, 20–26, 33–41) and (subsequent) blank runs with the conventional furnace heating program (steps 1–3, 11–19, 27–32, 42–50).

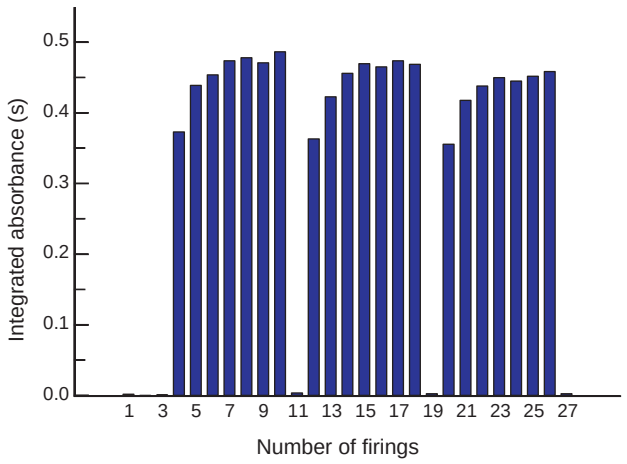

Fig. 6. Integrated absorbance signals of 1 μmol L^{-1} Er obtained with the conventional graphite furnace heating program (steps 4–9, 12–17, 20–25) and with the halocarbon-assisted program (steps 10, 18, 26), and subsequent blank runs with the conventional heating program (steps 11, 19, 27).

the three sets of runs is more considerable than in the case of the lower matrix concentration.

3.1.2.2. Bismuth tellurite. The memory signal of Er and Nd was also studied in the presence of Bi_2TeO_5. This matrix is rather volatile in the graphite furnace [11,27–31], so a lesser degree of memory effects would be expected for Er and Nd in its presence than in the presence of the $LiNbO_3$ matrix. Accordingly, the encountered first post-run memory signals were around 8–10% of the original Er signal, and showed a relatively faster decay than those in the case of $LiNbO_3$ (Figs. 3 and 5), but a more prolonged decay than those without matrix (Figs. 1 and 2). On the other hand, for Nd a quite large first post-run memory signal (10–15% of the original A_{int} signal) was achieved. This is likely due to the more serious memory of Nd with this particular matrix and the retaining of refractory oxides in the graphite furnace. These observations on slow evaporation of Er and Nd oxides are consistent with those made on the vaporization of REEs using ETAAS and ETV-coupled methods by Goltz et al. [22] and Byrne and Carambassis [23].

3.2. Vaporization studies with the halocarbon-assisted graphite furnace heating program

3.2.1. Vaporization of Er and Nd analytes without matrix

To overcome or at least decrease the memory effects described above, a modified graphite furnace program with an additional clean-out stage and dispension of CCl_4 was applied. Three measurement series of Er are depicted in Fig. 6. In each series, several subsequent measurements were performed with the conventional furnace heating program, and then the last measurement was made with the use of the furnace program extended with the CCl_4-assisted halogenation, followed by a blank run using again the regular heating program. The first measurement series started with a new pyrolytic graphite coated tube. As can be seen, these series show an increase of the Er signal in the subsequent measurements similarly to the case of Fig. 1, except that the memory signal decreases to a small value after the use of the halocarbon-assisted clean-out program. In the next measurement series (i.e., after the first use of halogenation), a stepwise increase of the Er signal can be seen at the beginning and the signal becomes constant after 3–4 subsequent runs. This stepwise absorbance increase is likely the consequence of the gradual removal of the chlorine containing compounds from the graphite tube in subsequent heating cycles, whose presence decrease the degree of the gas phase atomization of Er [11]. After the use of halocarbon assisted clean-out steps, the blank signals decrease to the level of A_{int}(blank) = 0.015–0.02 s, which is much less than A_{int}(blank) = 0.15 s, seen in Fig. 3. It is to be noted that the blank signal could be further decreased by the use of a higher vaporization temperature (e.g., 2200–2300 °C) in the clean-out program. However, this higher temperature could cause more erosion of the pyrolytic graphite coating and, as a consequence, faster aging of the graphite tube. When using the halocarbon-assisted program for Nd, similarly decreased memory effects were observed. Interestingly, the blank signal of Nd fluctuated more than that of Er.

3.2.2. Vaporization of Er and Nd in the presence of various matrices

The memory signal of Er in the presence of 0.001 mol L^{-1} $LiNbO_3$ was observed to be fairly decreasing (Fig. 7). However, the original value of the A_{int} signal was received only after a few regular runs. This can be due to the presence of residual chloride components of the matrix, remained in the furnace after halogenation, even after the regular post-runs. In the presence of 0.025 mol L^{-1} Bi_2TeO_5

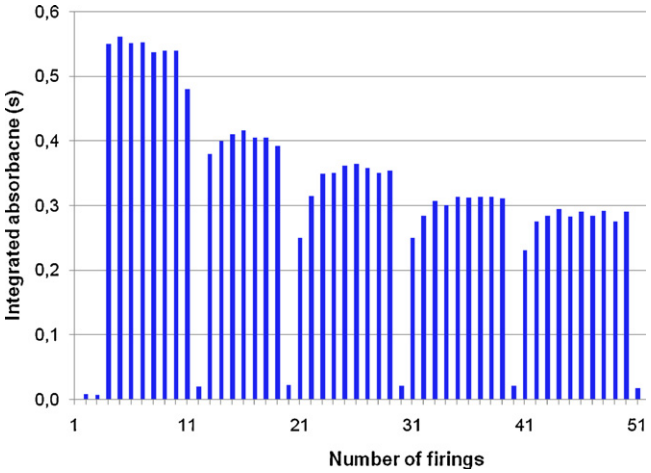

Fig. 7. Integrated absorbance signals of 1 μmol L^{-1} Er in the presence of 0.001 mol L^{-1} $LiNbO_3$ matrix, obtained with the conventional graphite furnace heating program (steps 4–10, 13–18, 21–28, 31–38, 41–49) and with the halocarbon-assisted program (steps 11, 19, 29, 39, 50), and subsequent blank runs with the conventional heating program (steps 12, 20, 30, 40, 51).

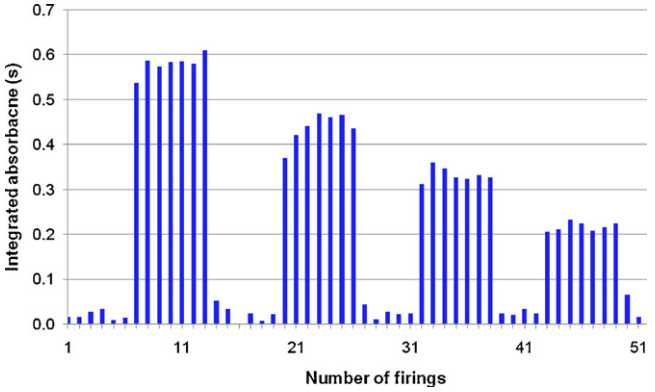

Fig. 8. Integrated absorbance signals of 10 μmol L^{-1} Nd in the presence of 0.0005 mol L^{-1} lithium niobate and 0.05 mol L^{-1} TAC obtained with the conventional graphite furnace heating program (steps 7–12, 20–25, 32–37, 43–48) and with the halocarbon-assisted program (steps 13, 26, 38, 49), and (subsequent) blank runs with the conventional heating program (steps 1–6, 14–19, 27–31, 39–42, 50–51).

matrix, the memory signal of Er still existed after the CCl_4-assisted cleaning, but diminished very quickly, e.g., within 1–2 firings.

For Nd in the presence of 0.025 mol L^{-1} Bi_2TeO_5 matrix, a rather efficient halogenation of the refractory sample components can be observed. However, the A_{int} signal for blank runs remains rather fluctuating. This behavior of Nd is similar as observed above for the case of Nd vaporized without any matrix and/or halogenation (e.g., Fig. 2). Interestingly, the A_{int} signal for the Nd standard reaches the maximum value within 1–2 post firings. A similar exponential behavior of the Nd memory signal with 0.0005 mol L^{-1} $LiNbO_3$, as for the case of Bi_2TeO_5 matrix, was experienced (Fig. 8). Moreover, a fairly faster deterioration of the Nd signal was observed in the presence of $LiNbO_3$ than in the presence of Bi_2TeO_5. This is likely due to the presence of matrix residues in the forms of their chlorides and/or oxychlorides, whose vaporization during the subsequent runs cause the erosion of the surface of the graphite tube. This consequently leads to a more pronounced loss of sensitivity. A partial solution to this problem can be the application of sample (matrix) dilution. These results all manifest that the halocarbon-assisted purification has limitations with the increasing mass and/or heavy volatility of the matrix-components. Therefore, for the efficient vaporization/halogenation of a matrix, it is necessary to optimize the amount of the CCl_4 residue by proper selection of the temperature and the length of the drying step in the cleaning sequence of the halocarbon-assisted graphite furnace heating program (Table 2).

3.3. Analytical curves and performance data

The calibration of Er and Nd was performed against simple aqueous solutions and as a comparison, against matrix-matched standards too. For calibrations on the base of A_p signals, the matrix-matching method had to be applied for attaining accurate results. Consequently, the application of A_{int} signal based calibration is recommended in routine analysis, for its simplicity. After each halocarbon-assisted purification step one blank run was performed to get rid of the residual chloride-compounds, preventing they could cause sensitivity decrease by signal suppression. The deterioration of the surface of the graphite tube (i.e., the gradual sensitivity decrease) was taken into account by resloping the calibration after the triplicate measurement of each sample.

Table 3
Analytical performance data of the ETAAS methods.

Parameter	ETAAS method	
	Conventional	CCl_4-assisted
Erbium; 0.1–1.5 μmol L^{-1} (n = 6)		
S_{int} (s L μmol^{-1})	0.850	0.760
S_p (L μmol^{-1})	0.624	0.516
LOD (μmol L^{-1})	0.020	0.017
LOD (μmol mol^{-1})	0.80	0.68
m_0 (pg)	16	18
Neodymium; 0.5–10 μmol L^{-1} (n = 5)		
S_{int} (s L μmol^{-1})	0.0619	0.0467
S_p (L μmol^{-1})	0.0442	0.0352
LOD (μmol L^{-1})	0.35	0.27
LOD (μmol mol^{-1})	14	11
m_0 (pg)	199	241

n – number of standards in the given concentration range, LOD – limit of detection, m_0 – characteristic mass, S_{int} and S_p – sensitivity (slope of the calibration curve) for A_{int} and A_p signals, respectively.

The sensitivities (slopes of the calibration curves) for A_p and A_{int} signals calculated with linear regression fittings to the calibration points are summarized in Table 3. Generally, the halocarbon-assisted methods showed a slightly lower sensitivity by 10–25% than the conventional ETAAS. Each calibration curve, irrespective of the analytes/methods, was characterized with a correlation coefficient (R) not worse than 0.9993. The limit of detection (LOD) data were generally found to be lower by 15% and 22% for Er and Nd, respectively, with the use of the halocarbon-assisted method than for the conventional ETAAS method, likely due to the lesser fluctuation occurring in the blank values. The characteristic mass (m_0) values were, however, higher by more than 10% for the halogen-assisted method. This was due to the residues of chloride compounds remaining in the tube after halogenation, which caused suppressed signals of Er and Nd in the subsequent analytical cycles. The halocarbon introduction also caused a relatively faster corrosion of the pyrolytic coating of the graphite tubes, which was manifest in a sensitivity decrease by the increasing number of the firings. This aging was considerably faster using the halocarbon-assisted cleaning than the conventional clean-out stage (e.g., 80–120 firings versus 150–200).

3.4. Comparison of analytical results

The applicability and accuracy of the halocarbon-assisted ETAAS method was tested by analyzing various crystal samples and the acquired results were compared with those obtained by the con-

Table 4
Comparison of the results of erbium and neodymium analysis in bismuth tellurite crystals obtained with ETAAS and XRF methods.

Crystal number	Crystal part	Added dopant concentration[a] (mmol/mol)	Measured concentration ± SD (mmol/mol)		
			Conventional ETAAS	CCl_4-assisted ETAAS	XRF
79506	M	1.0 (Er)	0.909 ± 0.031	0.890 ± 0.025	0.938 ± 0.048
	B		0.137 ± 0.010	0.129 ± 0.016	0.122 ± 0.051
	R		0.056 ± 0.002	0.055 ± 0.004	0.062 ± 0.027
79504	M	1.0 (Nd)	0.791 ± 0.023	1.016 ± 0.092	0.974 ± 0.090
	B		0.090 ± 0.003	0.092 ± 0.008	0.102 ± 0.041
	R		0.022 ± 0.002	0.029 ± 0.002	n.d.

[a] The concentration applied in the crystal growth melt, SD – standard deviation (n = 3), M – middle (upper), B – bottom, R – crystal growth residue, n.d. – not detected.

ventional ETAAS and XRF methods. According to the analytical results for A_{int} signal evaluation (Table 4), fairly good agreement was found between the dopant content of crystals determined by the conventional and the halocarbon-assisted ETAAS and the XRF methods, although the latter method generally exhibited higher RSDs. The dopant concentrations for both analytes show a decreasing trend from the top to the bottom of the crystal bulk, and also to the crystal growth residue. These important data correspond to a segregation coefficient in the crystals higher than unity for both dopant elements relative to the crystal growth melt.

4. Conclusions

Liquid carbon tetrachloride dispensed with a conventional autosampler into an end-heated graphite tube atomizer operated with an extended clean-out program was proven to be an effective halogenation technique to overcome memory effects arising from the insufficiently slow vaporization of refractory analytes and matrices. The increase in the analysis time of a complete heating cycle by applying the extended purification stage including the dispension of CCl_4 and the halogenation sequence is approximately 1 min. This duration is comparably much shorter than the application of multiple post-run blank firings in the case of a conventional graphite furnace heating program, which is necessary to get rid of the memory signals and carry-over. This novel halocarbon-assisted cleaning technique may be called as “fast heating induced impulse halogenation”.

It is to be noted that one can consider the applicability of the present halocarbon-assisted method to side-heated atomizers. These furnaces have a faster heating rate and a more homogeneous temperature profile [34] than end-heated furnaces, such as the one applied in the present study. Therefore, in a side-heated furnace generally the memory and carry-over effects are less pronounced than in an end-heated furnace, but still exist for example for Mo and V [29], which have similar tendency to form refractory compounds as REEs. Therefore, in the ETAAS analysis of all these elements by side-heated furnaces, the application of the present halocarbon-assisted cleaning technique could also be recommended.

It is to be mentioned that due to residual chlorine containing compounds in the graphite furnace after halogenation, a gradual sensitivity decrease was observed. This was likely due to the more serious deterioration of the graphite tube surface than under conventional graphite furnace heating cycles. This bias required the application of mathematical correction (resloping) of the calibration during the analysis. The effectiveness of the method was verified with the analysis of Er and Nd dopant elements in bismuth tellurite optical laser crystals.

The present in situ halogenation method is relatively simple, since it does not require any alteration in the graphite furnace gas supply system in contrast to most of the formerly introduced halogenation techniques. A further advantage of the halocarbon-assisted method maybe the possibility of its application to coupled ETV techniques to facilitate the low-temperature vaporization of medium volatile and refractory elements and to enhance their transport efficiency to the observation source.

Acknowledgements

The critical comments and advices of Prof. Tibor Kántor during this study and preparation of the manuscript are gratefully acknowledged. This work was supported by the Hungarian Scientific Research Fund (OTKA) under the project of F67647.

References

[1] T. Kántor, S.A. Clyburn, C. Veillon, Anal. Chem. 46 (1974) 2205–2213.
[2] B. Welz, G. Schlemmer, At. Spectrosc. 9 (1988) 81–83.
[3] B. Dočekal, V. Krivan, Anal. Chim. Acta 279 (1993) 253–260.
[4] E. Knutsen, G. Wibetoe, I. Martinsen, J. Anal. At. Spectrom. 10 (1995) 757–761.
[5] S. Scaccia, G. Zappa, Spectrochim. Acta B 55 (2000) 1271–1278.
[6] H.J. Heinrich, R. Matschat, Spectrochim. Acta B 62 (2007) 807–816.
[7] J.P. Matoušek, H.K.J. Powell, Spectrochim. Acta B 41 (1986) 1347–1355.
[8] J.P. Matoušek, R.T. Satumba, R.A. Bootes, Spectrochim. Acta B 44 (1989) 1009–1020.
[9] G.F. Kirkbright, R.D. Snook, Anal. Chem. 51 (1979) 1938–1941.
[10] T. Kántor, Fresenius J. Anal. Chem. 355 (1996) 606–614.
[11] L. Bencs, O. Szakács, T. Kántor, Spectrochim. Acta B 54 (1999) 1193–1206.
[12] T. Peng, X. Sheng, B. Hu, Z. Jiang, Analyst 125 (2000) 2089–2093.
[13] T. Peng, Z. Jiang, B. Hu, Z. Liao, Fresenius J. Anal. Chem. 364 (1999) 551–555.
[14] T. Peng, G. Chang, L. Wang, Z. Jiang, B. Hu, Fresenius J. Anal. Chem. 369 (2001) 461–465.
[15] D.L. Tsalev, V.I. Slaveykova, P.B. Mandjukov, Spectrochim. Acta Rev. 13 (1990) 225–274.
[16] D.L. Tsalev, V.I. Slaveykova, in: J. Sneddon (Ed.), Advances in Atomic Spectroscopy Volume IV, JAI Press Inc., Greenwich, Connecticut, 1998, pp. 27–150 (Chapter 2).
[17] T. Kántor, Spectrochim. Acta B 56 (2001) 1523–1563.
[18] H. Nickel, J.A.C. Broekaert, Fresenius J. Anal. Chem. 363 (1999) 145–155.
[19] L. Kovács, L. Rebouta, J.C. Soares, M.F. DaSilva, M. Hageali, J.P. Stoquert, P. Siffert, J.A. Sanzgarcia, G. Corradi, Zs. Szaller, K. Polgár, J. Phys. Condens. Matter 5 (1993) 781–794.
[20] I. Földvári, A. Munoz, E. Camarillo, Á. Péter, O. Szakács, Radiat. Eff. Def. Solids 149 (1999) 55–59.
[21] Z. Grobenski, Z. Fresenius, Anal. Chem. 289 (1978) 337–345.
[22] D.M. Goltz, D.C. Grégoire, C.L. Chakrabarti, Spectrochim. Acta B 50 (1995) 1365–1382.
[23] J.P. Byrne, A.L. Carambassis, Spectrochim. Acta B 51 (1996) 87–96.
[24] J.A. Holcombe, Spectrochim. Acta B 38 (1983) 609–615.
[25] I. Földvári, Á. Péter, R. Voszka, L.A. Kappers, J. Cryst. Growth 100 (1990) 75–77.
[26] K. Polgár, Á. Péter, L. Kovács, G. Corradi, Zs. Szaller, J. Cryst. Growth 177 (1997) 211–216.
[27] L. Bencs, O. Szakács, N. Szoboszlai, Zs. Ajtony, G. Bozsai, J. Anal. At. Spectrom. 18 (2003) 105–110.
[28] L. Bencs, O. Szakács, Spectrochim. Acta B 52 (1997) 1483–1496.
[29] L. Bencs, O. Szakács, T. Kántor, I. Varga, G. Bozsai, Spectrochim. Acta B 55 (2000) 883–891.
[30] L. Bencs, Magy. Kém. Foly. 106 (2000) 381–383.
[31] O. Szakács, L. Bencs, T. Kántor, I. Varga, G. Bozsai, Magy. Kém. Foly. 108 (2002) 84–92.
[32] B. Welz, M. Sperling, Atomic Absorption Spectrometry, 3rd ed., Wiley-VCH, Verlag GmbH, Weinheim, Germany, 1999.
[33] S.B. Smith, G.M. Hieftje, Appl. Spectrosc. 37 (1983) 419–424.
[34] M. Sperling, B. Welz, J. Hertzberg, C. Rieck, G. Marowsky, Spectrochim. Acta B 51 (1996) 897–930.